Towards High Resolution Trimming of Silicon Photonic Waveguides

April M. Logan, Xia Chen, Xingshi Yu, Weihong Shen, Xingzhao Yan, Weiwei Zhang, Goran Z. Mashanovich, Graham T. Reed, and David J. Thomson*

Optoelectronics Research Centre, University of Southampton, Southampton, United Kingdom
Email: aml4g19@soton.ac.uk

Funding: We acknowledge funding for HORIZON-EIC-2023 Pathfinder project DOLORES (101130178). D. J. Thomson acknowledges funding from the Royal Society for his University Research Fellowship (UF150325).

Keywords: Silicon Photonics, Phase Tuning, Programmable, Trimming, Ion Implantation

Abstract:

Methods for high resolution phase trimming of silicon Mach-Zehnder Interferometers via the electrical annealing of amorphized waveguide sections are presented. A high resolution of phase change is necessary to accurately trim the performance of individual devices to correct fabrication errors and when scaling to large programmable photonic circuits. On-chip microheaters positioned above amorphous waveguide sections are driven by short voltage pulses causing a degree of recrystallization, controllably changing the material's refractive index. An average resolution of phase change per voltage pulse of 0.0007π is demonstrated if an adaptive method is employed where the voltage step between successive pulses is set to be dependent on the average phase change brought about by the previous three voltage pulses.

1. Introduction

Photonic Integrated Circuits (PICs) contain a variety of photonic devices interconnected on a planar substrate to form a functional circuit. Their use has become increasingly popular in recent years driven by applications such as telecommunications [1-2], sensing [3], artificial intelligence [4-5] and quantum processing [6-7]. For communication applications, the use of light as a signal allows PICs to transmit vastly superior amounts of data at high speed compared to their electrical counterparts while maintaining low power consumption. Silicon based PICs are also attractive from a fabrication cost and integration perspective, benefiting from the mature semiconductor ecosystem developed over many years of electronic CMOS (Complementary Metal-Oxide Semiconductor) manufacturing.

As PICs become increasingly complex, a growing number of devices require trimming to correct phase errors resulting from fabrication imperfections [8,9]. This is particularly apparent in sub-micrometer silicon based waveguide platforms where the high index contrast means that any small imperfections or variations in waveguide dimensions can induce a large phase change in the waveguide, altering device characteristics substantially [8]. In most cases, trimming is currently implemented using on chip microheaters to electrically adjust the temperature of underlying waveguides resulting in a change in refractive index (and therefore change in phase of light) due to the thermo-optic effect [10]. However, each of these microheaters requires a non-insignificant amount of electrical power to be constantly applied, and thus with the ever-scaling number of components in increasingly complex PICs the total power consumption just for thermal trimming can become substantial. Alternative CMOS compatible and non-volatile methods for phase trimming where the characteristics of photonic devices can be permanently altered after fabrication and packaging are therefore highly attractive.

An additional strong motivation for the development of non-volatile post fabrication trimming is for the realization of low power programmable PICs. Commercialization of PICs has in part been limited by the long development cycle required to produce viable chips, including circuit (and potentially component) simulation and design, fabrication, and testing. This cycle can take upwards of a year [11] and may need to be repeated multiple times resulting in a high cost barrier particularly when producing at low volumes. To mitigate this issue, a multipurpose circuit that can be programmed to perform specific functions can be manufactured to produce off-the-shelf chips where simulation, design and fabrication have already happened,

significantly reducing development cycles. Programmable PICs therefore offer a large opportunity to expand the sector of silicon photonics.

Within programmable PICs, elements which can be controlled to selectively route the light to different functional devices are required to provide programmability. Essentially these elements are electro-optical switches where the incoming light can be passed to one or more waveguide paths. A popular implementation of this switching functionality within CMOS compatible programmable PICs is the use of a Mach-Zehnder interferometer (MZI) with a thermo-optic phase shifter. The power consumption of these thermo-optic elements is however again problematic, particularly as programmable PICs become more complex, and therefore low power non-volatile programmability is preferred.

Previous work has demonstrated that localized germanium ion implantation and subsequent annealing can be used to form trimmable and programmable non-volatile silicon photonic components [12-19]. When germanium ions are implanted into silicon waveguides, the collisions will cause defects and vacancies in the crystalline lattice structure which increases the refractive index of the silicon. When the lattice is close to 100% damaged it is considered to be amorphous, after which the refractive index of the silicon will not increase with further ion implantation. Amorphous silicon has a refractive index of approximately 3.96, whereas crystalline silicon has a refractive index of 3.48 at a wavelength of 1550nm [18]. The amorphized silicon can be recrystallized via annealing at temperatures above 450°C [17] which results in recovery of the refractive index. The amount of refractive index recovery is dependent on the anneal conditions (such as the time and temperature) and therefore the effective index of modes propagating within the implanted waveguide can be tuned through controlled annealing of the amorphized silicon.

Different implantation ions can be used to cause the lattice damage within the crystalline silicon waveguide, for this work germanium was chosen. The reasons for this are discussed in [18] and reiterated here for reference. Germanium and silicon are both Group IV elements, therefore the implantation of germanium ions will not introduce additional free carriers, avoiding a potential source of significant propagation loss within the waveguide. Furthermore, germanium has a higher relative mass than other ions within its group (such as carbon or silicon) and will therefore cause more lattice damage for a given implantation dose, which saves fabrication time and cost. Germanium is also a CMOS compatible material unlike other

materials used for making programmable PICs such as commonly used phase change materials. For germanium implanted silicon photonic circuits, the whole fabrication process is CMOS compatible.

Trimmable components such as MZIs, ring resonators and directional couplers can all be realized through the use of germanium ion implanted waveguides and subsequent annealing. These components can be tuned post-fabrication (and post-packaging) to correct performance or to route an optical signal down a specific path in a programmable PIC. Once the recrystallisation via annealing has taken place, it is however not possible to reintroduce the lattice damage hence realistically components can only be trimmed once; they are OTP (One Time Programmable). Tunable components created with germanium ion implantation and annealing are therefore best suited for circuits which need to be set in one configuration and then deployed. The components maintain their state after the removal of the electrical power used for annealing (they are non-volatile) and are therefore especially desirable for large scale circuits where the power consumption of individual components needs to be as low as possible.

The method of germanium ion implantation and annealing for programming offers low loss, as although implanted waveguides losses are approximately 32dB/mm [16] prior to annealing, sections as short as 12μm in length can provide a 2π phase shift, corresponding to a loss of approximately 0.4dB. Beyond that, as annealing is occurring, the propagation loss through the implanted waveguide will decrease because the 32dB/mm loss is due by the lattice damage within the silicon. Losses caused by germanium absorption can be considered negligible due to the low implant dose used (meaning the concentration level of germanium implanted within the waveguide is nominal), further information on this can be found in [16].

To begin the recrystallisation process in the implanted waveguide, and thereby change the refractive index of implanted sections post fabrication, different methods of localized annealing can be used. Laser annealing is an effective method [14], however this cannot be conducted after packaging and requires a specialized laser set up. An alternative as investigated in this work, is to use on-chip microheaters fabricated above the implanted waveguides to anneal electrically. By passing electrical current through the microheater, its filament will increase in temperature (Joule heating) and as it reaches temperatures over 450°C the lattice damage will begin to repair, thus reducing the refractive index as the silicon

recrystallizes [17]. After a device has been annealed, the thermal stability overtime is important. If a device is only partially annealed, exposing it to a temperature higher than the one it was originally annealed at would further anneal the device, leading to a shift away from the desired phase. For the majority of applications this is not a concern as normal operating temperatures should fall well below the temperature required for annealing to take place, which is at minimum 450°C.

The microheaters required for electrical annealing are essentially the same as the standard microheaters utilized for thermo-optic tuning within PICs but are around an order of magnitude shorter due to the large change in refractive index possible when annealing. Therefore, these microheaters are available as a part of most silicon photonic foundry services. The loss introduced by these microheaters is also negligible as they are separated from the waveguide by a silicon oxide cladding layer (explained in more detail in Section 2). For a programmable circuit to be desirable to a wide market, setting the state of components must be possible after packaging, indicating that electrical annealing is most viable for this application. A further benefit of electrically annealing is the possibility to trim multiple devices in parallel, reducing the time it takes to program a full-scale circuit.

While previous work has demonstrated that on-chip microheaters can be used to electrically anneal and recrystallize amorphized regions [17-19], the annealing process has not been deeply studied to investigate the resolution of phase trimming possible. Here, the use of short electrical pulses to progressively anneal a section of amorphized waveguide within one arm of an MZI is investigated. Pulses were used as opposed to applying a constant voltage they offer a gradual and controllable annealing process which can provide a higher resolution of phase change. High resolution is particularly important when trimming large scale programmable circuits as phase errors would cause an additive error as the light propagates through multiple components. The use of pulses for annealing also offers the ability to monitor the device transmission between each partial anneal, as the waveguide can be given time to cool, meaning the device characteristics are not influenced by the thermo-optic effect and will therefore be in their normal operating state. Different approaches to set the voltage of the pulses throughout the annealing process are investigated here with the aim to find out which provides the highest accuracy of phase trimming whilst maintaining efficiency. In other words, the high resolution must be achievable in the minimal amount of applied voltage pulses. Aside from phase resolution, the method must also be repeatable between multiple

devices and have a phase trimming range of at least 2π to allow photonic devices to be trimmed to any desired transmission state.

The results show that the highest resolution of phase change resulted from an adaptive approach which relied on real-time feedback of the degree of phase change produced by previous pulses to set the voltage of the next pulse in the sequence. This achieved an average resolution of 0.0007π per voltage pulse. The utilization of real-time feedback allows the annealing cycle to be kept efficient, such that when in the cycle the annealing effect is low, larger voltage steps can be used. Real-time feedback aids repeatability between devices due to the annealing process for each device being tailored to that device's behavior. The electrical power of the pulses required for annealing ranged from approximately 35mW at the start of the anneal process to 110mW for full annealing. The actual power required for a specific device will therefore depend on where in the 2π range the device needs to be trimmed to.

2. MZI design and fabrication

MZIs were primarily used in this work as a tool to develop the annealing method as they allow accurate measurement of the phase shift produced via trimming. They additionally offer a starting point from which a programmable PIC can be developed. MZIs are commonly used components within optical circuits. Within an MZI, input light is split into two waveguide paths before being recombined. The relative phase of light from the two paths dictates the degree of coupling to two output waveguides from the combiner. If light is fully outputted from one output waveguide, a π phase shift will cause the light to be completely switched to the other output waveguide [20]. MZIs therefore offer a way to switch and route optical signals, as well as being useful for applications where modulation, filtering and sensing are required. 2×2 symmetrical MZIs were used in this work, formed with rib waveguides of width 450nm, thickness 220nm and a slab height of 110nm. Symmetric MZIs were used as they offer greater stability to global temperature changes as both arms are of equal length and have the same thermal based refractive index change (so the phase shift in each arm induced by a global temperature change will cancel out). Therefore, global temperature fluctuations will not influence the phase change measured.

Figure 1 shows schematic illustrations of the device design and cross-section, as well as an optical microscope image of the fabricated MZI. The upper arm of the MZI contains a 12μm long germanium ion implanted section of waveguide with a microheater filament positioned

above it. A length of 12µm was chosen for the implanted waveguide to ensure that a tuning range of at least 2π is possible. A microheater with a filament width of 1µm is centered over the implanted waveguide, and extends beyond the implanted region by 1µm lengthways. The filament of the microheater is formed of titanium nitride, with vias and pads made of aluminum. To limit absorption of the light from the waveguide by the titanium nitride filament, a 400nm thick silicon dioxide cladding layer was deposited between the filament and the top of the implanted waveguide. The silicon dioxide layer reduces the efficiency of the microheater to an extent as silicon dioxide has a lower thermal conductivity than silicon, however, because these devices do not require a constant power to maintain their state once they have been trimmed/programmed, this is not a major concern. Further along the upper arm of the MZI, there is a second microheater with a filament length of 200µm and filament width of 1 µm. This microheater is used to form a thermal tuner, and the waveguide below it is not implanted (it is crystalline silicon).

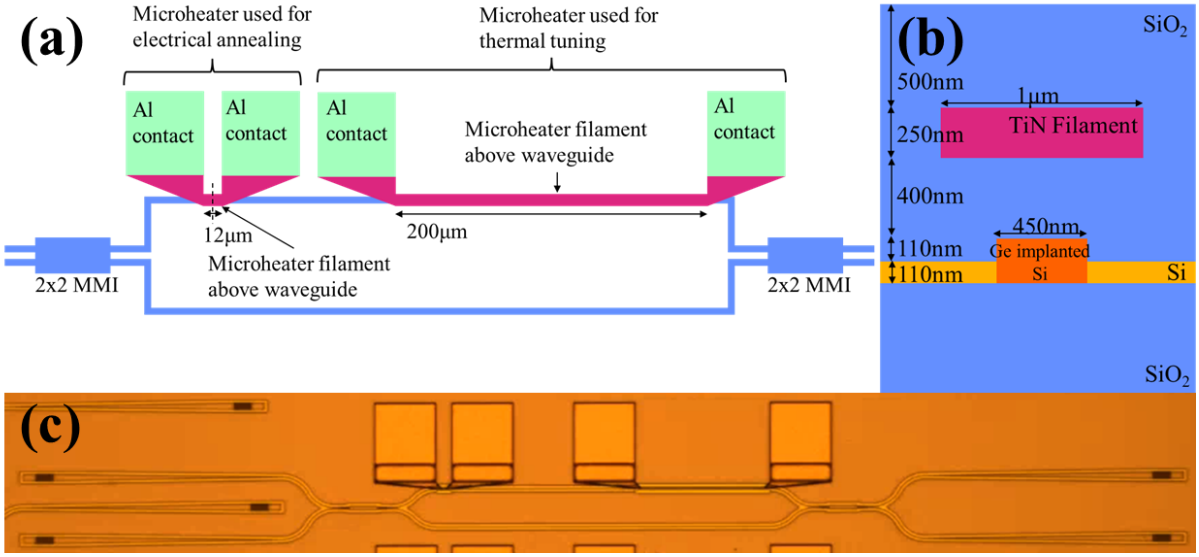

Figure 1: (a) Diagram of the MZI configuration, (b) Cross-section diagram of the germanium implanted region of waveguide, where the dotted line is displayed on Figure 1a, (c) Microscope image of one of the fabricated MZIs.

The MZI fabrication was conducted within the University of Southampton Nanofabrication Cleanrooms, excluding germanium ion implantation which took place at the University of Surrey Ion Beam Centre. For the fabrication, a SOI (Silicon on Insulator) wafer with a 2µm thick buried silicon dioxide layer and silicon overlayer of thickness 220nm was used. The wafer was patterned with DUV (Deep Ultra-Violet) lithography throughout the fabrication process. ICP (Inductive Coupled Plasma) etching was used to form the grating couplers (70nm etch) and etch the rib waveguides (110nm etch). After this a 300nm silicon dioxide

layer was deposited via PECVD (Plasma-Enhanced Chemical Vapor Deposition) and etched via ICP etching to create a hardmask. This hardmask covered the entire wafer excluding the sections of waveguide that needed to be exposed during the ion implantation. For the implantation, a dose of 1×10^{15} ions/cm^2 and an energy of 135keV were used. After the implantation, the hardmask was removed using hydrofluoric (HF) acid etching. The next part of the fabrication process was to form the microheaters. To do this, the rib waveguides were encapsulated with a 400nm layer of silicon dioxide deposited via PECVD. The wafer was then patterned for the formation of the filaments. Titanium nitride was deposited via sputtering and then the wafer underwent a liftoff process to remove the excess metal. This involved immersing the wafer in edge bead removal solvent 70/30 and later isopropyl alcohol. During the immersion, the beaker containing the wafer and solvent was placed in an ultrasonic tank heated to 60°C and sonicated. Before forming the vias, a further 500nm of silicon dioxide was deposited on the wafer above the filament layer using PECVD. Lithography was then used to define the position of vias which were etched down to the filament layer using HF. To fill the vias with metal and to create the electrode pads of the microheaters, the wafer was patterned with the layout of the electrode pads, and an aluminum layer was deposited over the wafer. To finish the fabrication process, a further liftoff process was necessary to remove the excess aluminum.

3. Experimental methods and results

Different methods of electrical annealing with voltage pulses were experimentally investigated. To determine the overall resolution of each method (and therefore find a way to achieve a high resolution of trimming) it is necessary to calculate the phase change induced by each voltage pulse during the annealing process. In order to do this, during the annealing cycle after each voltage pulse was applied the optical transmission through the device at 1550nm was measured. These values for optical transmission were fitted to a MZI model and using the change in transmission between adjacent values it was possible to determine the change in phase induced by that voltage pulse. To ensure the model could accurately determine the phase shift, the MZI was set to the quadrature point before the annealing cycle was started. This was done by applying a voltage sweep to the second microheater (shown in Figure 1 as the microheater for thermal tuner) to determine the minimum and maximum in transmission, and also the voltage required for a 50:50 transmission to the two outputs of the MZI. This voltage was then held on the thermal tuner throughout the annealing process.

Multiple methods of electrical annealing were tested where different voltage pulse durations and voltage steps were used. The results from selected key methods are summarized in **Table 1**.

Table 1: Summary of phase change per voltage source for different electrical annealing methods.

Electrical annealing method	Average resolution of phase change per voltage pulse (π rad)	Standard deviation of phase change over an entire annealing cycle (π rad)	Largest phase change measured (π rad)
Pulse width 1s with a constant step of 100mV	0.10	0.14	0.54
Pulse width 50ms with a constant step of 100mV	0.07	0.11	0.52
Pulse width 50ms with a constant step of 25mV	0.01	0.02	0.12
Step falling between 17mV to 100mV, dependent on electrical power across the filament (50ms pulse width)	0.03	0.07	0.46
Adaptive step dependent on phase (50ms pulse width)	0.0007	0.0006	0.0054

The first two methods compare pulse durations of 50ms and 1s. For both, the step in voltage between each pulse was 100mV. In Table 1, it can be observed that the shorter pulse duration results in both a smaller average phase change per pulse and a smaller standard deviation, indicating that shorter pulse widths have both a higher resolution and more repeatable annealing result pulse to pulse. The third method described in the table uses a smaller voltage step than the previous methods, allowing for a comparison between voltage steps of 100mV and 25mV for a fixed pulse duration of 50ms. Using a small voltage step again results in both a smaller average phase change and smaller standard deviation.

The first three methods lead to the interpretation that the shortest pulse width and smallest voltage step would provide the highest resolution of phase trimming, however these methods do not delve into the efficiency of the annealing (achieving a high resolution with the minimum number of applied voltage pulses). The forth method was developed to investigate a

potential avenue for improving efficiency. This method examines whether it is better to have a voltage step that corresponds to a linear step in electrical power, which should more closely produce a linear increase in temperature from pulse to pulse. The average resolution and standard deviation achieved from this method are higher than for the fixed 25mV voltage step. However, for this method the voltage step decreases during the annealing cycle and therefore the annealing can become more efficient as it involves applying a larger voltage step at lower temperatures, where the degree of annealing per pulse is lower, thus accelerating the annealing process. At higher temperatures where annealing occurs rapidly, the step between adjacent pulses is lower to maintain resolution. Therefore, although this method ultimately does not provide a solution for achieving a high resolution of phase trimming, it demonstrates that using a varying voltage step can provide higher efficiency.

Generally, through annealing multiple devices using variations of the methods discussed above, it was found that smaller steps (which provide a smaller temperature increase between pulses) and shorter pulse widths cause less of an annealing effect, which was expected [15]. This implies that the highest resolution of phase tuning per pulse would require an annealing cycle of many short pulses with a minimal step increase between adjacent pulses. The downside to this approach would be that it results in a long and inefficient process which maybe undesirable, particularly if a large number of devices need to be trimmed. Another important finding was not from the four methods already discussed, but instead from continually annealing with multiple pulses at the same voltage. When applying these repeated pulses of the same voltage, annealing would eventually saturate as the temperature threshold to anneal the implanted waveguide any further would be higher. As such it was determined it would be necessary to have an increase in voltage during the annealing cycle to dissipate additional electrical power across the filament and ensure the annealing temperature continuously increased until the device fully annealed.

These findings led to the final ‘adaptive step’ method discussed in Table 1, which relies on real-time feedback of the phase change brought about by previous voltage pulses to select what voltage step should be taken next. This method was developed to enable both a high resolution demonstrated by using a 50ms pulse with the smallest step size, and the increase in efficiency that was shown by the varying step size of the electrical power dependent method. For this method, the optical measurements carried out after each voltage pulse were used to calculate the phase change brought about by the annealing due to that pulse. From this the

average phase change produced by the previous three voltage pulses could be determined (referred to from here as Δφ) and then compared to the thresholds in **Table 2** for selection of the subsequent voltage step. To determine the threshold values that are presented in Table 2, an optimization process was carried out by annealing multiple devices with varying thresholds for each step, until values were found that would provide efficient and high resolution annealing. During the annealing cycle, to preserve a high resolution of phase trimming control, there was potential for the voltage level to remain equal or even reduce in magnitude for the following pulse, in order to decelerate the rate of phase change. To make the process more time efficient a large voltage step was implemented where the degree of annealing was minimal. For the majority of the annealing cycle, Δφ fell within the thresholds that corresponded to a 0.6mV step, which was the minimum resolution of the voltage source being used to apply the electrical signal. The actual power dissipated across the annealing filament was further minimized through the use of an external series resistance connected between the device under test and the voltage source. The microheater filament had an approximate resistance of 280Ω, and the external resistance was approximately 438Ω, meaning that approximately 40% of the power of each pulse contributed to annealing the implanted waveguide.

Table 2: Voltage steps applied dependent on previous phase change.

Average phase change of the previous three voltage pulses, Δφ (radians)	Voltage step used next (mV)
Δφ >0.012	-1.2
0.012 > Δφ > 0.006	0
0.006 > Δφ > 0.001	0.6
0.001> Δφ	10

Figure 2 contains the data collected during the electrical annealing cycle using the adaptive phase dependent step method. From the y-axis of Figure 2a, it can be observed that annealing begins at a pulse voltage of around 3.2V, and ends at 5.8V, which correspond to electrical powers applied across the microheater of approximately 35mW and 110mW respectively. Figure 2b shows the accumulative change in phase over the entire annealing cycle, which reached approximately 2π. For applications where a larger tuning range is required, the length of the germanium implanted section of waveguide could be increased. Figure 2c displays the phase shift induced by each voltage pulse. The highest phase change brought about by a

single pulse was 0.0054π, however in most cases the phase change between successive pulses falls below half of this maximum value. Figure 2d is a histogram of the data from Figure 2c, which further illustrates this. For this adaptive method, the average phase change per pulse was 0.0007π, signifying that a high resolution of phase change per pulse is achievable with this method of post-fabrication trimming. For all methods a total phase change of at least 2π was achieved during the annealing process. Considering the 12μm length of implanted waveguide this corresponds to a total phase change per micron of 0.16π to 0.2π.

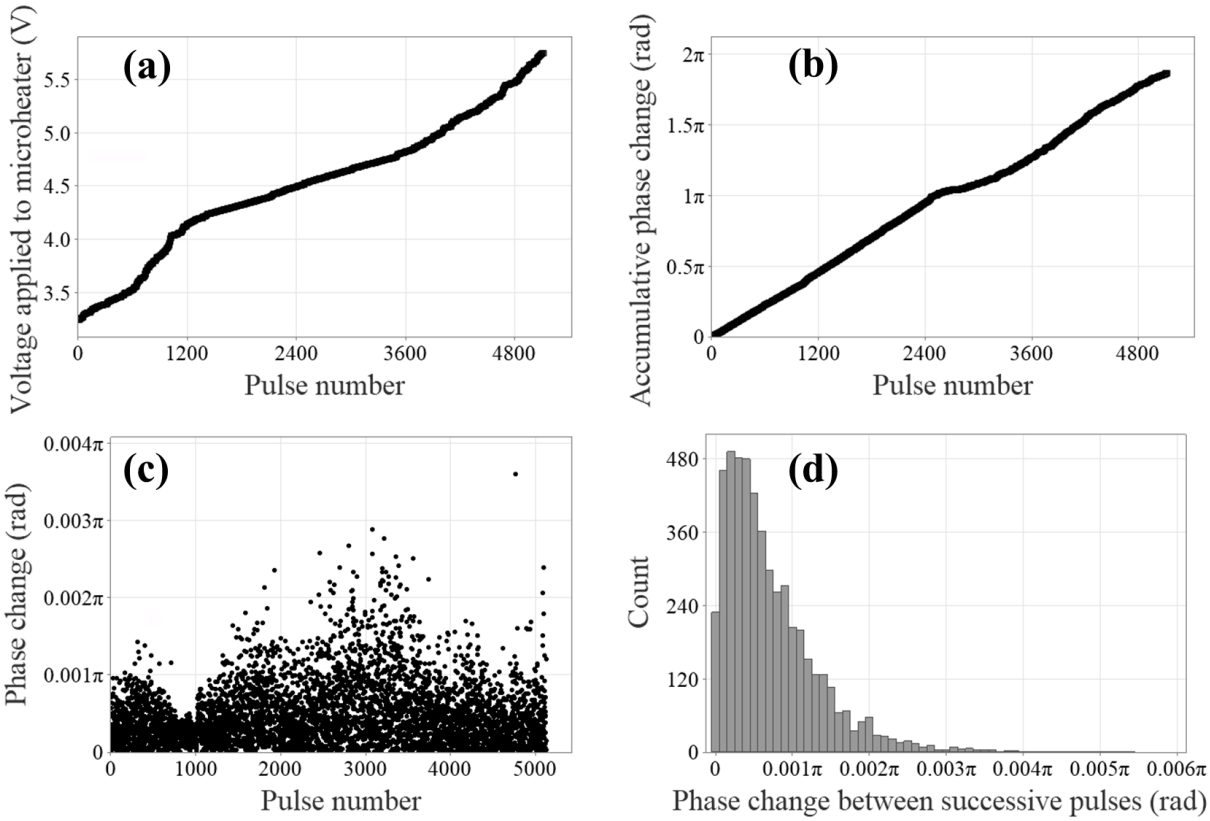

Figure 2: (a) Pulse voltage applied across the filament during the annealing cycle, (b) Accumulative phase change induced by electrical annealing over the entire annealing cycle, (c) Phase change measured between successive pulses, (d) Histogram of data from Figure 2c.

4. Conclusion and further work

A variety of different electrical pulse annealing recipes for phase trimming of germanium implanted MZIs have been investigated, with the aim of developing a method that could provide efficient, high resolution phase tuning. The experiment established that shorter voltage pulse widths lead to a higher resolution, so for the optimized method, a 50ms pulse width was used. Another factor that improved resolution was to use small voltage steps,

however it was determined that in order for the annealing to be efficient as well as have a high resolution, some sort of variation in voltage step across the annealing cycle was necessary. This led to the development of a method which was found to provide the highest resolution of phase change per voltage pulse in the minimum number of voltage pulses, which relied on real-time feedback where the step between adjacent voltage pulses was dependent on the average phase change brought about by the previous three voltage pulses. With this method, the average phase change per pulse achieved was 0.0007π, indicating this method could provide a high accuracy of phase trimming. The most essential factor for achieving the high resolution is the real-time feedback of monitoring the optical transmission during the annealing cycle. **Table 3** contains a comparison of this method to other methods in the literature for trimming germanium ion implanted waveguides.

Table 3: Comparison of tuning methods for germanium implanted waveguides.

	Device	Type of annealing	Type of trimming	Power required to fully anneal the device	Phase accuracy achieved
[14]	MZI	Continuous wave laser	Scanning a laser spot across the implanted waveguide	45mW per 0.5μm length of implanted waveguide	0.025π
[19]	RR	Electrical via on chip microheater (tungsten filament)	Pulses width modulated voltage	525mW	<0.01π
This work	MZI	Electrical via on chip microheater (titanium nitride filament)	Voltage pulses with an adaptive voltage step	110mW	At minimum 0.0054π, average of 0.0007π

In order to fully anneal the devices in this work, a power of 110mW is required, however the energy consumption necessary will depend on the resolution of phase trimming required. Nevertheless, the implanted waveguides are non-volatile and thus do not need a constant power to maintain their state once trimmed. This makes this technique desirable for large scale PICs in applications where they only need to be trimmed once before deployment. Now that a sufficient level of precision has been achieved, work is underway to realize mesh circuits that utilize germanium ion implantation and annealing for programming via phase trimming to demonstrate viability for larger scale programmable photonic circuits using this

technique. The technique is also being used to demonstrate the viability of low power resonant optical switching circuits via precise trimming.

Acknowledgements

We acknowledge funding for HORIZON-EIC-2023 Pathfinder project DOLORES (101130178). D. J. Thomson acknowledges funding from the Royal Society for his University Research Fellowship (UF150325).

Data Availability Statement

The data that support the findings of this study are openly available in Pure at https://doi.org/10.5258/SOTON/D3504, reference number [21].

Received: ((will be filled in by the editorial staff))
Revised: ((will be filled in by the editorial staff))
Published online: ((will be filled in by the editorial staff))

References

1. N. Margalit, et al., "Perspective on the future of silicon photonics and electronics," Applied Physics Letters 118, 220501 (2021). 10.1063/5.0050117
2. S. Shekhar, et al., "Roadmapping the next generation of silicon photonics," Nat Commun 15, 751 (2024). 10.1038/s41467-024-44750-0
3. M. Iqbal, et al., "Label-free biosensor arrays based on silicon ring resonators and high-speed optical scanning instrumentation," IEEE Journal of Selected Topics in Quantum Electronics 16,. 654-661 (2010). 10.1109/JSTQE.2009.2032510.
4. Y. Shen, et al., "Deep learning with coherent nanophotonic circuits," Nature Photonics 11, 441-446 (2017). 10.1038/nphoton.2017.93
5. B. Bai, et al., "Microcomb-based integrated photonic processing unit" Nature Communications 14, 66 (2023). 10.1038/s41467-022-35506-9.
6. N. C. Harris, et al., "Large-scale quantum photonic circuits in silicon," Nanophotonics 5, 456-468 (2016). 10.1515/nanoph-2015-0146
7. J. Notaros, et al., "Programmable dispersion on a photonic integrated circuit for classical and quantum applications," Opt. Express 25, 21275-21285 (2017) 10.1364/OE.25.021275
8. W. A. Zortman, et al., "Silicon photonics manufacturing," Optics Express 18, 23598-23607 (2010). 10.1364/OE.18.023598

9. T. Zhongyu, et al., “Ultralow Loss Coupling Tuning of Photonic Accelerators,” Advanced Photonics Research 2500175, (2025). 10.1002/adpr.202500175

10. J. Sun, et al., “A 128 Gb/s PAM4 Silicon Microring Modulator with Integrated Thermo-Optic Resonance Tuning,” Journal of Lightwave Technology 37, 110-115 (2019). 10.1109/JLT.2018.2878327

11. W. Bogaerts and A. Rahim, “Programmable Photonics: An Opportunity for an Accessible Large-Volume PIC Ecosystem,” IEEE Journal of Selected Topics in Quantum Electronics 26 (2020). 10.1109/JSTQE.2020.2982980

12. R. Loiacono, et al., “Laser erasable implanted gratings for integrated silicon photonics,” Optics Express 19, 10728-10734 (2011). 10.1364/OE.19.010728

13. R. Topley, et al., “Locally Erasable Couplers for Optical Device Testing in Silicon on Insulator,” Journal of Lightwave Technology 32, 2248-2253 (2014). 10.1109/JLT.2014.2324018

14. X. Chen, et al., “Post-fabrication phase trimming of Mach-Zehnder interferometers by laser annealing of germanium implanted waveguides,” Photonics Research 5, 578-582 (2017). 10.1364/PRJ.5.000578

15. M. M. Milosevic, et al., “Ion Implantation in Silicon for Trimming the Operating Wavelength of Ring Resonators,” IEEE Journal of Selected Topics in Quantum Electronics 24(2018). 10.1109/JSTQE.2018.2799660

16. X. Chen, et al., “Silicon erasable waveguides and directional couplers by germanium ion implantation for configurable photonic circuits,” Optics Express 28, 17630-17642 (2020). 10.1364/OE.394871

17. X. Yu, et al., “Electrically Erasable Optical I/O for Wafer Scale Testing of Silicon Photonic Integrated Circuits,” IEEE Photonics Journal 12(2020). 10.1109/JPHOT.2020.3027799

18. X. Yu, et al., “Ge Ion Implanted Photonic Devices and Annealing for Emerging Applications,” Micromachines 13(2022). 10.3390/mi13020291

19. H. Jayatilleka, et al., “Post-Fabrication Trimming of Silicon Photonic Ring Resonators at Wafer-Scale,” Journal of Lightwave Technology 39, 5083-5088 (2021). 10.1109/JLT.2021.3079801

20. A. Lui, et al, “Silicon photonics: the state of the art”, Wiley, Chapter 7 (2008). 10.1002/9780470611142.

21. A. M. Logan, “Towards high resolution trimming for silicon photonic waveguides,” University of Southampton, (2025). 10.5258/SOTON/D3504